A discrete-fibers model for bridged cracks and reinforced elliptical voids

K. Bertoldi[a], D. Bigoni[b,*], W.J. Drugan[b,1]

[a]Department of Mechanical Engineering, Massachusetts Institute of Technology, Cambridge, MA, USA
[b]Dipartimento di Ingegneria Meccanica e Strutturale, Università di Trento, Via Mesiano 77, I-38050 Trento, Italy

Abstract

A model of crack bridging and reinforced elliptical voids is proposed, in which the fibers joining the surfaces of the void or crack are modelled as discrete, linear elastic bars. We show that a theory recently developed by us to analyze structural interfaces permits analytical attack and solution of multiple important previously unsolved problems of stress concentration and fracture. In particular, an analytical solution is provided for a reinforced elliptical void, which, by superposition, allows treatment of arbitrary fiber distributions, which can be even randomly distributed and oriented. In the special case of small or null ratio between a void's axes, new stress intensity factor expressions are obtained, which account for fibers' inclination and geometry.
© 2006 Elsevier Ltd. All rights reserved.

Keywords: Fracture mechanics; Mechanical interfaces; Elliptical reinforced voids; Structural interfaces; Reinforced cracks

1. Introduction

In fiber-reinforced materials, such as short-glass-fiber-reinforced polypropylene (Fig. 1), fibers joining the surfaces of cracks or voids are usually observed. These fibers strongly

---

*Corresponding author. Tel.: +39 0461 882507; fax: +39 0461 882599.

E-mail addresses: bertoldk@mit.edu (K. Bertoldi), davide.bigoni@ing.unitn.it (D. Bigoni), drugan@engr.wisc.edu (W.J. Drugan).

URL: http://www.ing.unitn.it/~bigoni/.

[1]Permanent address: Department of Engineering Physics, 1500 Engineering Drive, University of Wisconsin-Madison, Madison, WI 53706, USA.

influence the stress distribution and provide important stress relief. The quantification of the stress redistribution due to the presence of the fibers and the evaluation of the relevant stress intensity factors have been the focus of a number of studies. Initially, crack bridging was modelled by Rose (1987) as a continuous distribution of springs, a model thoroughly analyzed by Movchan and Willis (1993, 1996, 1997). However, the discrete nature of the bridging is of fundamental importance, so that Meda and Steif (1992) considered the case of one fiber bridging the crack, focusing on the fiber slipping along its interface, and Rubinstein (1994) analyzed a crack reinforced by discrete fibers *orthogonal* to the crack. However, multiple important aspects remain unaddressed, namely the effects of inclined reinforcing fibers on a crack under both Modes I and II loading, and of general reinforcing fibers on an elliptical void. The present article addresses these issues.

Fibers bridging the surfaces of a crack or an elliptical void represent an example of a *structural interface* and can therefore be analyzed within the framework given by Bigoni and Movchan (2002) and Bertoldi et al. (2007a, b). We show that for two-dimensional linear elasticity, it is possible to solve the case of an elliptical void in an infinite sheet, subject to arbitrary uniform stress at infinity, when a *generic* geometry of fibers (with linear behavior) are bridging the surfaces of the void. In the limiting case when an axis of the ellipse is either small or is reduced to zero, the ellipse becomes either a bridged thin void or a bridged crack. In these cases we derive the relevant stress intensity factors. For fibers orthogonal to the crack surface, we provide rigorous proof that a single fiber (of appropriate stiffness) at the crack tip causes the stress intensity factor to vanish, a situation consistent with results from the Dugdale–Barenblatt model (Dugdale, 1960; Barenblatt, 1962). Moreover, consideration of *fiber inclination*, not previously studied, allows us to quantify new effects, as for instance the optimal fiber distribution and orientation to minimize the stress intensity factors under both Modes I and II loading.

2. Elliptical voids reinforced by bridging fibers

Our study of crack bridging and toughening of brittle materials with fibers is initiated in this section by addressing the problem of an elliptical hole in an infinite linearly elastic sheet deformed in plane strain or plane stress, reinforced with discrete linear fibers and loaded by a remote, uniform loading. As illustrated in Fig. 2, let us denote by $\partial\Omega$ the boundary of an elliptical void in an infinite sheet (having Lamé moduli λ and μ and loaded

Fig. 1. A bridged fracture in short-glass-fiber-reinforced polypropylene.

at infinity by a uniform loading) and with ω_j the jth junction between fibers and the continuous body on $\partial\Omega$. At a junction, the load is transmitted as if the fibers were a 'linear, filamentary structure' connecting the junctions of central points $\mathbf{x}_h$ and $\mathbf{x}_j$, defined by the direction specified by the unit vector $\mathbf{e}_{(hj)}$

$$\mathbf{e}_{(hj)} = \frac{\mathbf{x}_h - \mathbf{x}_j}{|\mathbf{x}_h - \mathbf{x}_j|}. \tag{1}$$

At the jth junction where M different fibers converge, the traction $\mathbf{t}^j$ transmitted to the infinite matrix is a linear function of the displacement difference $\mathbf{u}(\tilde{\mathbf{x}}) - \mathbf{u}(\mathbf{x})$ between points $\tilde{\mathbf{x}}$ and $\mathbf{x}$ of the opposite junctions ω_h and ω_j

$$\mathbf{t}^j(\mathbf{x}) = \sum_{h=1}^{M} k_{(hj)}[(\mathbf{u}(\tilde{\mathbf{x}}) - \mathbf{u}(\mathbf{x}))\cdot\mathbf{e}_{(hj)}]\mathbf{e}_{(hj)}, \quad \mathbf{x} \in \omega_j, \ \ \tilde{\mathbf{x}} \in \omega_h, \tag{2}$$

where $k_{(hj)}$ denotes the stiffness of the filament hj.

The stress field $\boldsymbol{\sigma}$ in the infinite matrix (in the absence of body forces) satisfies

$$\begin{cases} \text{div } \boldsymbol{\sigma}(\mathbf{x}) = \mathbf{0}, & \mathbf{x} \in \text{infinite sheet}, \\ \boldsymbol{\sigma}(\mathbf{x})\mathbf{n}(\mathbf{x}) = \sum_{h=1}^{M} k_{(hj)}[(\mathbf{u}(\tilde{\mathbf{x}}) - \mathbf{u}(\mathbf{x}))\cdot\mathbf{e}_{(hj)}]\mathbf{e}_{(hj)}, & \mathbf{x} \in \omega_j, \ \ \tilde{\mathbf{x}} \in \omega_h, \\ \text{uniform stress applied at infinity}, \end{cases} \tag{3}$$

where $\mathbf{n}$ is the outward unit normal to the elliptical void boundary. Note that the displacements, and therefore the tractions transmitted by the fibers to the infinite matrix at the junctions, have an initially unknown distribution.

Problem (3) is an example of a multistructure (see Kozlov et al., 1999 and references cited therein); a simplification of it is pursued here by working with averaged quantities at the junctions between the fibers and the infinite matrix, as explained in detail by Bertoldi et al. (2007a). Briefly, we introduce the averaged tractions and displacements at junctions as

$$\bar{\mathbf{t}}_j = \frac{1}{|\omega_j|} \int_{\omega_j} \mathbf{t}(\mathbf{x}) = \mathbf{t}(\mathbf{x}_j) + O(|\omega_j|^2), \quad \bar{\mathbf{u}}_j = \frac{1}{|\omega_j|} \int_{\omega_j} \mathbf{u}(\mathbf{x}) = \mathbf{u}(\mathbf{x}_j) + O(|\omega_j|^2), \tag{4}$$
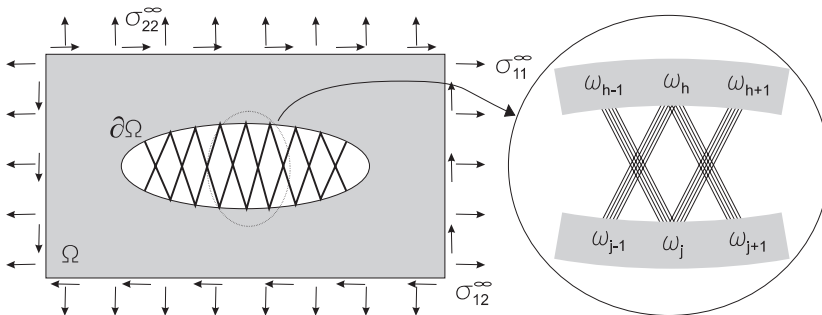
Fig. 2. Elliptical hole in a plane linearly elastic infinite sheet reinforced with discrete linear fibers and loaded by a remote, uniform loading.

so that the boundary value problem (3) is replaced by

$$\begin{cases} \operatorname{div} \boldsymbol{\sigma}(\mathbf{x}) = \mathbf{0}, & \mathbf{x} \in \text{infinite sheet}, \\ \boldsymbol{\sigma}(\mathbf{x})\mathbf{n}(\mathbf{x}) = \sum_{h=1}^{M} k_{(hj)}[(\mathbf{u}(\mathbf{x}_h) - \mathbf{u}(\mathbf{x}_j)) \cdot \mathbf{e}_{(hj)}]\mathbf{e}_{(hj)}, & \mathbf{x} \in \omega_j, \\ \text{uniform stress applied at infinity,} \end{cases} \qquad (5)$$

where the initially unknown traction distributions over the junctions are replaced by uniform distributions, calculated as linear functions of the displacement differences at the central points $\mathbf{x}_h$ and $\mathbf{x}_j$ of opposite junctions ω_h and ω_j.

Problem (5), replacing the more difficult problem (3),[2] is employed as the basis for analyzing an elliptical void reinforced by fibers. We proceed as follows:

- The solution in the infinite sheet for uniform traction distributions over the junction regions ω_j is constructed (via Muskhelishvili–Kolossoff complex potentials), so that the displacements at the junction points $\mathbf{u}(\mathbf{x}_h)$ are written as functions of the (for the moment unknown) uniform tractions $\mathbf{t}(\mathbf{x}_h)$ applied at joint regions and of the remote applied stress.
- Since a displacement/force relationship is now known at each junction, the structure representing the fibers is solved as a linear structure on elastic supports via the usual methods of structural mechanics.

The problem of an infinite elastic sheet with an elliptical void reinforced by linear fibers is attacked by employing the Muskhelishvili–Kolossoff (Muskhelishvili, 1953) complex potentials $\phi(z)$ and $\psi(z)$. In terms of these potentials, the general solution to plane equilibrium problems for homogeneous, isotropic linear elastic materials can be expressed in polar components as

$$2\mu(u_r + \mathrm{i}u_\theta) = \mathrm{e}^{-\mathrm{i}\theta}[\kappa\phi(z) - z\overline{\phi'(z)} - \overline{\psi(z)}],$$

$$\sigma_{rr} + \sigma_{\theta\theta} = 4\operatorname{Re}[\phi'(z)],$$

$$\sigma_{\theta\theta} - \sigma_{rr} + 2\mathrm{i}\sigma_{r\theta} = 2\mathrm{e}^{2\mathrm{i}\theta}[\bar{z}\phi''(z) + \psi'(z)], \qquad (6)$$

where $z = x_1 + \mathrm{i}x_2 = r\mathrm{e}^{\mathrm{i}\theta}$, prime denotes derivative with respect to a function's argument, overbar denotes complex-conjugate, $\kappa = 3 - 4v$ for plane strain and $\kappa = (3 - v)/(1 + v)$ for plane stress, and μ and v are the elastic shear modulus and the Poisson ratio, respectively.

In order to analytically solve the problem of an infinite elastic sheet with an elliptical void reinforced by linear fibers, we need some preliminary results. These are the two solutions corresponding to

- An elliptical hole in an infinite elastic sheet, loaded by a remote uniform stress. Employing the conformal mapping

$$z = \omega(\zeta) = R\left(\zeta + \frac{m}{\zeta}\right), \qquad (7)$$

---

[2]Assuming that the size of the junction zones is small when compared to the dimension of the void, so that these zones 'contract' onto the points $\mathbf{x}_j$, it has been shown in Appendix A of Bertoldi et al. (2007a) that the elastic energy evaluated by solving (3) differs from that evaluated by solving (5) by terms of $O(|\omega_j|^2)$.

where

$$R = \frac{a+b}{2}, \quad m = \frac{a-b}{a+b}, \tag{8}$$

that conformally maps the infinite matrix with an elliptical void of semi-axes a and b into an infinite matrix with a circular void of unit radius, it can be shown that the solution of the problem is given by (Muskhelishvili, 1953)

$$\phi(\zeta) = \Gamma_1 R \left(\zeta - \frac{m}{\zeta} \right) - \frac{\overline{\Gamma}_2 R}{\zeta},$$

$$\psi(\zeta) = \Gamma_2 R \zeta - \frac{\Gamma_1 R}{\zeta} - \frac{R}{\zeta(\zeta^2 - m)} [\overline{\Gamma}_2 + m\Gamma_1 + (\Gamma_1 + m\overline{\Gamma}_2 + 2m^2\Gamma_1)\zeta^2], \tag{9}$$

with

$$\Gamma_1 = \frac{\sigma_{11}^\infty + \sigma_{22}^\infty}{4}, \quad \Gamma_2 = \frac{\sigma_{22}^\infty - \sigma_{11}^\infty}{2} + i\sigma_{12}^\infty. \tag{10}$$

- A self-equilibrated but otherwise arbitrary distribution of uniform loadings acting on separated portions of an elliptical hole in an infinite elastic sheet. The solution for an infinite matrix containing an elliptical hole on which N piecewise uniform traction distributions having normal and tangential components p_k and s_k act on the parts $\widehat{z_k^- z_k^+}$, see Fig. 3 (with null total resultant) is given by Bertoldi et al. (2007a)

$$\phi(\zeta) = -\frac{1}{2\pi i} \sum_{k=1}^{N} (p_k + is_k) \left\{ R \left[\sigma_k^+ - \sigma_k^- - \frac{m}{\zeta} \log\frac{\sigma_k^+}{\sigma_k^-} + \left(\zeta + \frac{m}{\zeta} \right) \right. \right.$$
$$\left. \left. \times \log\left(\frac{\sigma_k^+ - \zeta}{\sigma_k^- - \zeta} \right) \right] + z_k^- \log(\sigma_k^- - \zeta) - z_k^+ \log(\sigma_k^+ - \zeta) \right\},$$

$$\psi(\zeta) = -\frac{1}{2\pi i} \sum_{k=1}^{N} (p_k - is_k) \left\{ R \left[m\sigma_k^+ - m\sigma_k^- - \frac{1}{\zeta} \log\frac{\sigma_k^+}{\sigma_k^-} + \left(m\zeta + \frac{1}{\zeta} \right) \right. \right.$$
$$\left. \left. \times \log\left(\frac{\sigma_k^+ - \zeta}{\sigma_k^- - \zeta} \right) \right] + \overline{z}_k^- \log(\sigma_k^- - \zeta) - \overline{z}_k^+ \log(\sigma_k^+ - \zeta) \right\} - \frac{\zeta(1 + m\zeta^2)}{\zeta^2 - m} \phi'(\zeta), \quad (11)$$
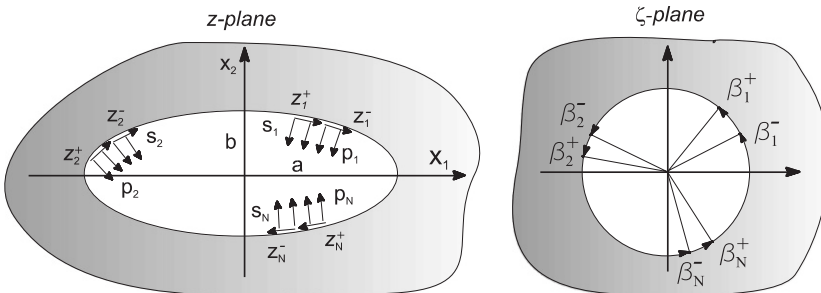
Fig. 3. Elliptical hole in an infinite elastic matrix with N applied uniform normal and tangential traction distributions in the z-plane, and its conformal mapping in the ζ-plane.

where the polar form for ζ is used

$$\zeta = \rho e^{i\beta}, \tag{12}$$

so that $\sigma_k^- = e^{i\beta_k^-}$ and $\sigma_k^+ = e^{i\beta_k^+}$ denote points on the circular void of unit radius $\rho = 1$, again having employed the conformal mapping (7) with (8).

Employing solutions (9)–(11), the displacements at the junction points $\mathbf{u}(\mathbf{x}_h)$ are written as functions of the (for the moment unknown) uniform tractions $\mathbf{t}(\mathbf{x}_h)$ (having normal and tangential component p_k and s_k, respectively) applied at joint regions and of the applied remote stress:

$$
\begin{aligned}
u_1(e^{i\beta}) + iu_2(e^{i\beta}) = {} & \frac{(1+\kappa)Re^{-i\beta}}{8\mu}\left\{4i\sigma_{12}^\infty + \sum_{\alpha=1}^{2}[e^{2i\beta} - m - 2(-1)^\alpha]\sigma_{\alpha\alpha}^\infty\right\} \\
& + \sum_{k=1}^{N}\sum_{\alpha=1}^{2}\frac{i(p_k + is_k)R}{4\pi\mu}(-1)^\alpha\left\{\frac{i}{2}(1+\kappa)\left(e^{i\beta} - \frac{m}{e^{i\beta}}\right)\beta_{k\alpha}\right. \\
& + \frac{\kappa+1}{2}\left(e^{i\beta} + \frac{m}{e^{i\beta}} - e^{i\beta_{k\alpha}} - \frac{m}{e^{i\beta_{k\alpha}}}\right)\log[1 - \cos(\beta_{k\alpha} - \beta)] \\
& \left. - i(\kappa - 1)\left(e^{i\beta_{k\alpha}} + \frac{m}{e^{i\beta_{k\alpha}}}\right)\arg(e^{i\beta_{k\alpha}} - e^{i\beta})\right\},
\end{aligned}
\tag{13}
$$

where $\beta_{k1} = \beta_k^-$, $\beta_{k2} = \beta_k^+$.

Eq. (13) provides the relation between applied tractions and the resulting displacements at the junctions; with this relation any linear elastic structure connecting the junctions can be solved as a linear structure on elastic supports.

As a first example, we consider an infinite matrix with an elliptical void characterized by $a/b = \frac{5}{2}$ and reinforced by fibers characterized by a nondimensionalized thickness $t_b/a = \frac{1}{1000}$. The dimensionless fiber compliance parameter introduced by Rubinstein (1994)

$$\Lambda = \frac{2\mu}{(\kappa + 1)kt_b}, \tag{14}$$

is employed, which is null (infinite) when fibers are rigid (have vanishingly small stiffness). A uniform uniaxial stress $\sigma_{22}^\infty = \mu/100$ is applied at infinity. The largest stress concentration, namely, σ_{22} at point A, is plotted in Fig. 4 as a function of the fibers, inclination α (see detail in Fig. 4) for a hole reinforced by six fibers. It can be seen from the figure that the stress concentration decreases as a function of the fiber inclination and reaches a minimum for fibers having an inclination near $\alpha = 80°$ (depending on the Λ value).

In Fig. 5, the level sets of the von Mises stress, defined as

$$\sigma_{VM} = \sqrt{[(\sigma_1 - \sigma_2)^2 + (\sigma_1 - \sigma_3)^2 + (\sigma_3 - \sigma_2)^2]/2}, \tag{15}$$

with σ_i denoting the principal stresses, are plotted in a region near the elliptical void (note that σ_{VM} has been normalized by the remote stress) for both Mode I loading (left) and Mode II loading (right). The fibers are characterized by an inclination $\alpha = 80°$ and a compliance $\Lambda = 1$; the number of fibers N has been taken equal to $\{0, 6, 12, 24\}$.
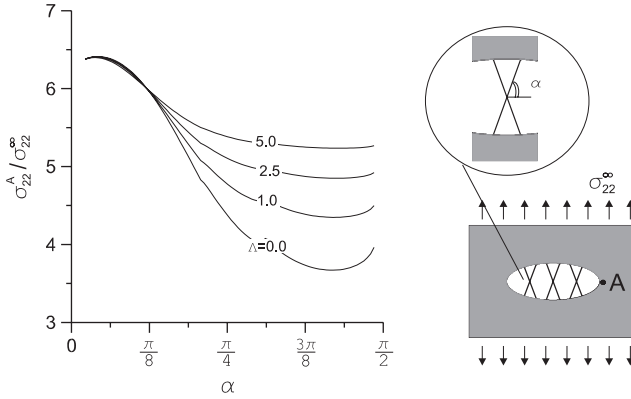
Fig. 4. Stress concentration (at point A) for an elliptical void ($a/b = \frac{5}{2}$) reinforced by six fibers and loaded under uniaxial (vertical) stress, as a function of the fibers' inclination α. Different values of the fiber compliance parameter Λ are considered.

As a second example, we consider the same elliptical void just analyzed, but with 8, 16 and 32 randomly disposed fibers. Mode I loading is shown at left and Mode II at right in Fig. 6, for the same fiber distributions.

3. Elliptical thin voids reinforced by bridging fibers

In order to determine the stress field near the tip of an elliptical thin void (having semi-axes b and a, with $b \ll a$), a coordinate system is introduced having the origin at a distance $\rho/2$ from the void end, as shown in Fig. 7, where ρ denotes the radius of curvature at the end ($\theta = 0$)

$$\rho = \frac{b^2}{a}. \tag{16}$$

Regarding the thin void as a crack having a finite tip radius, two loading systems are considered (Fig. 7): one symmetric (representing Mode I loading) and one skew-symmetric (representing Mode II loading) with respect to the two axes x_1 and x_2. Employing this setting, and expanding in Taylor series the solution (given by Eq. (11), see also Appendix C of Bertoldi et al., 2007a) for the infinite matrix with an elliptical hole loaded as in Fig. 7 near $\rho = 0$ and near $r = 0$, we obtain the leading-order terms of the displacement and stress fields near the crack tip (for $b/a \ll 1$) in terms of stress intensity factors K_{I} and K_{II}

- Mode I

$$u_1 = \frac{K_{\mathrm{I}}}{2\mu} \sqrt{\frac{r}{2\pi}} \cos\frac{\theta}{2} \left(\kappa - 1 + 2\sin^2\frac{\theta}{2} + \frac{\rho}{r} \right),$$

$$u_2 = \frac{K_{\mathrm{I}}}{2\mu} \sqrt{\frac{r}{2\pi}} \sin\frac{\theta}{2} \left(\kappa + 1 - 2\cos^2\frac{\theta}{2} + \frac{\rho}{r} \right),$$
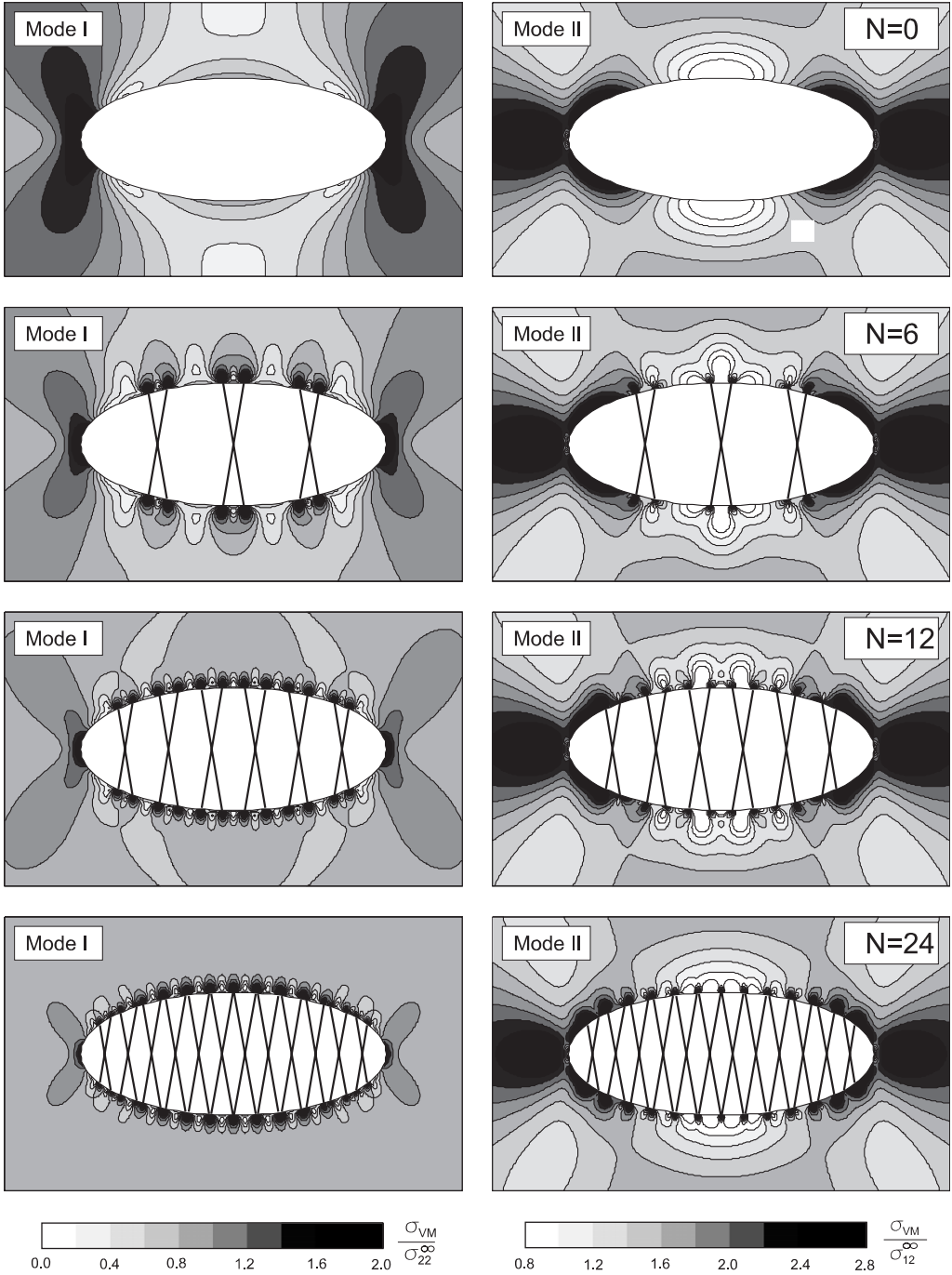
Fig. 5. Von Mises stress (normalized by remote stress) for an elliptical void ($a/b = \frac{5}{2}$) reinforced by N fibers, loaded by a uniform remote uniaxial vertical stress σ_{22}^{∞} (left) and a uniform remote shear stress σ_{12}^{∞} (right). The fibers are characterized by an inclination $\alpha = 80°$ and a compliance $\Lambda = 1$.
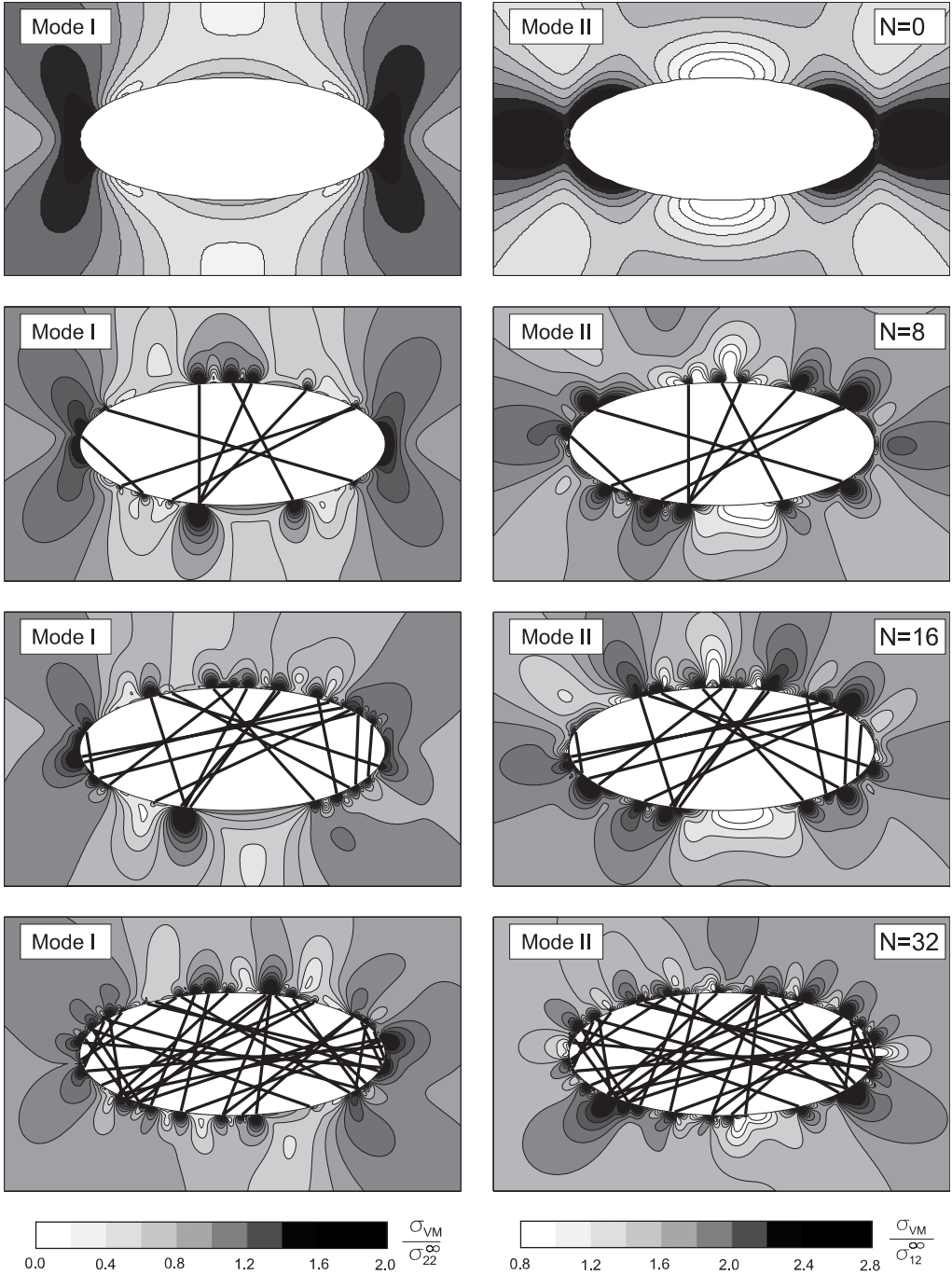
Fig. 6. Von Mises stress distribution (normalized by remote stress) for an infinite matrix with an elliptical void ($a/b = 5/2$) reinforced by N randomly disposed fibers, loaded by a uniform remote uniaxial vertical stress σ_{22}^{∞} (left figures) and a uniform remote shear stress σ_{12}^{∞} (right figures). The fibers are characterized by $\Lambda = 1$.
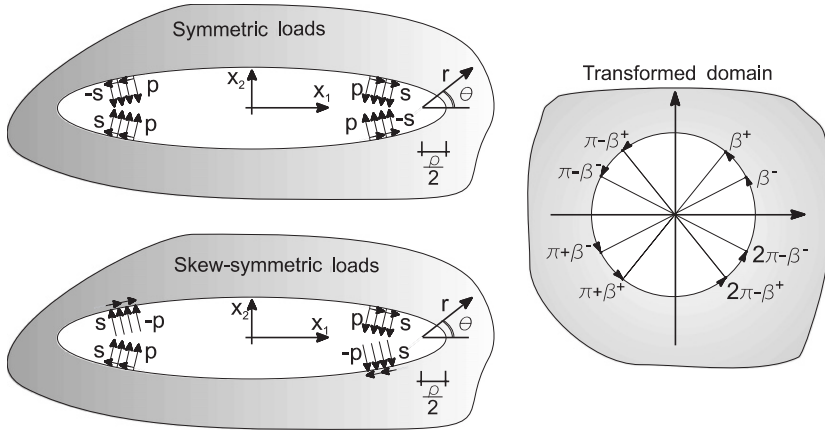
Fig. 7. Coordinate system for determination of stress field near the tip of an elliptical void.

$$\sigma_{11} = \frac{K_{\mathrm{I}}}{\sqrt{2\pi r}} \left[\cos\frac{\theta}{2} \left(1 - \sin\frac{\theta}{2}\sin\frac{3\theta}{2} \right) - \frac{\rho}{2r}\cos\frac{3\theta}{2} \right],$$

$$\sigma_{12} = \frac{K_{\mathrm{I}}}{\sqrt{2\pi r}} \left(\sin\frac{\theta}{2}\cos\frac{\theta}{2}\cos\frac{3\theta}{2} - \frac{\rho}{2r}\sin\frac{3\theta}{2} \right),$$

$$\sigma_{22} = \frac{K_{\mathrm{I}}}{\sqrt{2\pi r}} \left[\cos\frac{\theta}{2} \left(1 + \sin\frac{\theta}{2}\sin\frac{3\theta}{2} \right) + \frac{\rho}{2r}\cos\frac{3\theta}{2} \right]. \tag{17}$$

- Mode II

$$u_1 = \frac{K_{\mathrm{II}}}{2\mu}\sqrt{\frac{r}{2\pi}}\sin\frac{\theta}{2}\left(\kappa + 1 + 2\cos^2\frac{\theta}{2} - \frac{\rho}{2} \right),$$

$$u_2 = \frac{K_{\mathrm{II}}}{2\mu}\sqrt{\frac{r}{2\pi}}\cos\frac{\theta}{2}\left(1 - \kappa + 2\sin^2\frac{\theta}{2} + \frac{\rho}{2} \right),$$

$$\sigma_{11} = \frac{K_{\mathrm{II}}}{\sqrt{2\pi r}} \left[-\sin\frac{\theta}{2}\left(2 + \cos\frac{\theta}{2}\cos\frac{3\theta}{2} \right) + \frac{\rho}{2r}\sin\frac{3\theta}{2} \right],$$

$$\sigma_{12} = \frac{K_{\mathrm{II}}}{\sqrt{2\pi r}} \left[\cos\frac{\theta}{2}\left(1 - \sin\frac{\theta}{2}\sin\frac{3\theta}{2} \right) - \frac{\rho}{2r}\cos\frac{3\theta}{2} \right],$$

$$\sigma_{22} = \frac{K_{\mathrm{II}}}{\sqrt{2\pi r}} \left(\sin\frac{\theta}{2}\cos\frac{\theta}{2}\cos\frac{3\theta}{2} - \frac{\rho}{2r}\sin\frac{3\theta}{2} \right). \tag{18}$$

Creager and Paris (1967) report an identical asymptotic representation for the stress field. In addition to the asymptotic representation (17) and (18), our solution also gives the values of the stress intensity factors. These are the following functions of the loading

distribution, with normal and tangential components p and s, applied on the boundary portions delimited in the transformed domain by the angles $[\beta^-, \beta^+]$, $[\pi - \beta^+, \pi - \beta^-]$, $[\pi + \beta^-, \pi + \beta^+]$ and $[2\pi - \beta^+, 2\pi - \beta^-]$ (Fig. 7)

$$K_{\mathrm{I}} = -\frac{2p\sqrt{a}}{\sqrt{\pi}}(\beta^+ - \beta^-), \quad K_{\mathrm{II}} = 0, \tag{19}$$

$$K_{\mathrm{I}} = 0, \quad K_{\mathrm{II}} = \frac{2s\sqrt{a}}{\sqrt{\pi}}(\beta^+ - \beta^-), \tag{20}$$

for symmetric and skew-symmetric traction distributions, respectively.

In the limiting case of concentrated loads with normal and tangential components P and S applied at points defined in the transformed domain by the angles β, $\pi - \beta$, $\pi + \beta$ and $2\pi - \beta$, Eqs. (19) and (20) reduce to

$$K_{\mathrm{I}} = -\frac{2P}{\sqrt{a\pi}\sin\beta}, \quad K_{\mathrm{II}} = 0 \tag{21}$$

and

$$K_{\mathrm{I}} = 0, \quad K_{\mathrm{II}} = \frac{2S}{\sqrt{a\pi}\sin\beta}, \tag{22}$$

respectively.

As an example, we consider the fiber geometries shown in Fig. 8 for an ellipse with $a/b = 20$ and junctions characterized by $|\omega|/a = \frac{1}{1000}$. The inclined fibers are oriented at an angle of $5°$ with respect to the horizontal direction. For the arrangements considered $\beta = \pi/3$, so that the four junctions central points in the transformed domain are defined by the angles $\{\pi/3, 2\pi/3, 4\pi/3, 5\pi/3\}$, whereas the (finite-width) junctions are delimited in the transformed domain by the angular ranges $[1.0466, 1.0478]$, $[2.09382, 2.09497]$, $[4.18821, 4.18937]$ and $[-1.0478, -1.0466]$. Therefore, from Eqs. (19) and (20), we obtain

$$K_{\mathrm{I}} = -0.0058208p, \quad K_{\mathrm{II}} = 0.0058208s, \tag{23}$$

whereas considering the resultant force of p and s, respectively, $P = p|\omega|$ and $S = s|\omega|$, concentrated in the junction center, we can employ Eqs. (21) and (22) to get

$$K_{\mathrm{I}} = -0.291346P = -0.0058232p, \quad K_{\mathrm{II}} = 0.291346S = 0.0058232s, \tag{24}$$

values that are very close to those given by Eq. (23).
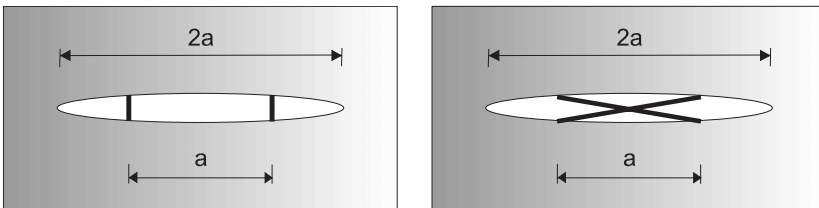
Fig. 8. Two fiber geometries with vertical and inclined (at $5°$ with respect to the horizontal direction) fibers.

3.1. Elliptical thin void reinforced by two central inclined fibers

We analyze the influence of reinforcing fibers' inclination on the stress intensity factor, by considering an elliptical void of semi-axes a and b (with $a \gg b$) reinforced by two central fibers inclined at an angle α with respect to the horizontal direction (see detail in Fig. 9). In this case, the tractions transmitted by the fiber to the matrix are related to the fiber elongation as

$$p\cos(\theta^{\mathbf{n}} - \alpha) - s\sin(\theta^{\mathbf{n}} - \alpha) = 2k[U_1\cos\alpha + U_2\sin\alpha], \quad 0 \leqslant \beta \leqslant \frac{\pi}{2}, \tag{25}$$

where $\theta^{\mathbf{n}}$ denotes the angle between the unit inward (pointing towards the matrix) normal and the x_1-axis at the fiber central point, and the displacement at the fiber central point $\mathbf{U}$ is the sum of the displacements produced by the remote loading $\mathbf{u}^\infty$ and by the (distribution of four) normal p and tangential s tractions acting on the junctions

$$\mathbf{U} = \mathbf{u}^\infty + p\mathbf{u}^p + s\mathbf{u}^s. \tag{26}$$

In addition, since the force transmitted at each node of the elastic matrix has the same inclination as the fiber, its normal and tangential components are related through

$$s = -p\tan(\theta^{\mathbf{n}} - \alpha). \tag{27}$$

Substitution of Eqs. (26) and (27) into Eq. (25) yields

$$p = \frac{2k\cos(\theta^{\mathbf{n}} - \alpha)(u_1^\infty\cos\alpha + u_2^\infty\sin\alpha)}{1 - 2kt_b\cos(\theta^{\mathbf{n}} - \alpha)[u_1^p\cos\alpha + u_2^p\sin\alpha - \tan(\theta^{\mathbf{n}} - \alpha)(u_1^s\cos\alpha + u_2^s\sin\alpha)]}. \tag{28}$$

As an application, we have considered an elliptical thin void characterized by $a/b = 20$ and $t_b/a = \frac{1}{1000}$. The stress intensity factors K_{I} and K_{II} (normalized by $\sigma_{22}^\infty\sqrt{\pi a}$ and $\sigma_{12}^\infty\sqrt{\pi a}$, respectively) are reported in Fig. 9 versus the fibers' inclination angle α, for different values of the dimensionless fiber compliance parameter Λ.

Several features may be observed from Fig. 9. In particular:

- For Mode I loading (left in the figure), the normalized stress intensity factor assumes values above unity (meaning that the fiber-reinforced elliptical void results in a higher
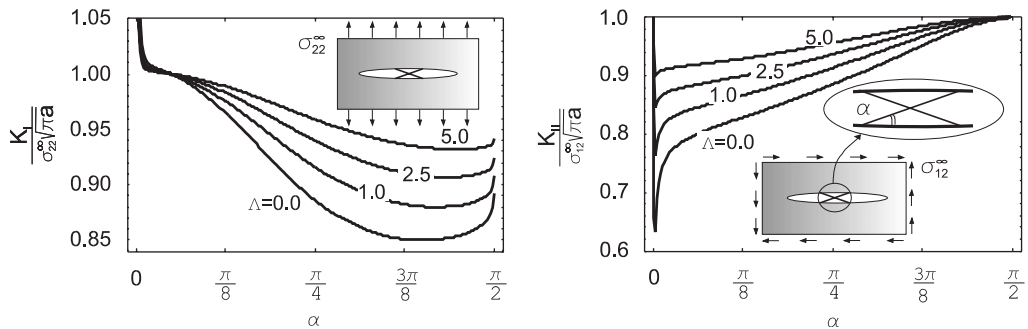
Fig. 9. Stress intensity factor K_{I} (normalized by $\sigma_{22}^\infty\sqrt{\pi a}$, on the left) and K_{II} (normalized by $\sigma_{12}^\infty\sqrt{\pi a}$, on the right), for an elliptical void ($a/b = 20$) reinforced by two central inclined fibers for different values of the fiber compliance parameter Λ as function of the fiber inclination α.

stress concentration than the unreinforced void) for nearly horizontal fibers; this is due to the Poisson effect, since nearly-horizontal fibers are compressed, thus increasing K_I.

- Also for Mode I loading, K_I decreases as a function of the fiber inclination and reaches a minimum for fibers having an inclination near $\alpha = 3\pi/8 = 67.5°$ (depending on the Λ value).
- For Mode II loading (right in the figure), vertical ($\alpha = \pi/2$) or horizontal ($\alpha = 0$) fibers remain unloaded and therefore are ineffective in reducing K_{II}.
- Also for Mode II loading, the stress intensity factor undergoes a sudden drop for nearly horizontal fibers and then increases with the fiber inclination angle α. The minimum K_{II} is attained for fibers having an inclination near $\alpha = 0.5°$.

From the above features we note that it is possible to combine nearly horizontal and nearly vertical fibers to produce an 'optimal' reinforced void (assuming centrally-located fibers). In particular, for $\Lambda = 1$, we find that

$$\sqrt{K_I^2/(\sigma_{22}^\infty \sqrt{\pi a})^2 + K_{II}^2/(\sigma_{12}^\infty \sqrt{\pi a})^2} \tag{29}$$

is minimum when the elliptical void is reinforced by two fibers inclined at 2° with respect to the horizontal direction and two fibers at 65°, as shown in Fig. 10. (We further find these optimal fiber angles to be little changed for all hole aspect ratios $a/b > 15$.) For this fiber arrangement the dimensionless stress intensity factor K_I is equal to 0.91 whereas K_{II} is equal to 0.77.

3.2. Elliptical thin voids reinforced with generic structures

To explore the effects of fiber morphology and distribution, an elliptical void is considered having the high aspect ratio $a/b = 20$, so that the geometry approaches that of a crack, bridged by different arrangements of fibers. In particular, two arrangements of fibers are considered: purely vertical and inclined. The latter has been defined in such a way as to provide the same vertical stiffness given by vertical fibers, with a double Warren truss structure with fibers inclined at 30° with respect to the vertical (see the detail in Fig. 11). The fibers are characterized by $\Lambda = 0.075$ for the vertical case and $\Lambda = 0.075(4\cos^2\pi/6) = 0.225$ for the inclined case. An elastic matrix is considered, characterized by $\nu = 0.3$, and separately subjected to uniform uniaxial stress $\sigma_{22}^\infty = \mu/100$ and shearing stress $\sigma_{12}^\infty = \mu/100$ at infinity.

The stress intensity factor is plotted as a function of fiber density $N/(2ac)$ in Fig. 11, ranging between 0 and 25 for the vertical fiber model and 0 and 100 for the inclined fiber model. It is assumed that the fibers join the crack faces within the segment $(1 - c)\,a \leqslant |x_1| \leqslant a$ (see details in Fig. 11). Three different situations are considered: $c = 1$
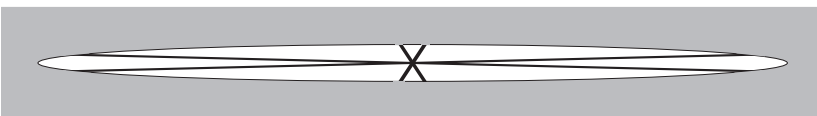
Fig. 10. Fiber reinforcement of an elliptical void ($a/b = 20$) with centrally located fibers permitting minimization of both Modes I and II stress intensity factors. Fibers are inclined at 2° and 65° with respect to the horizontal direction.
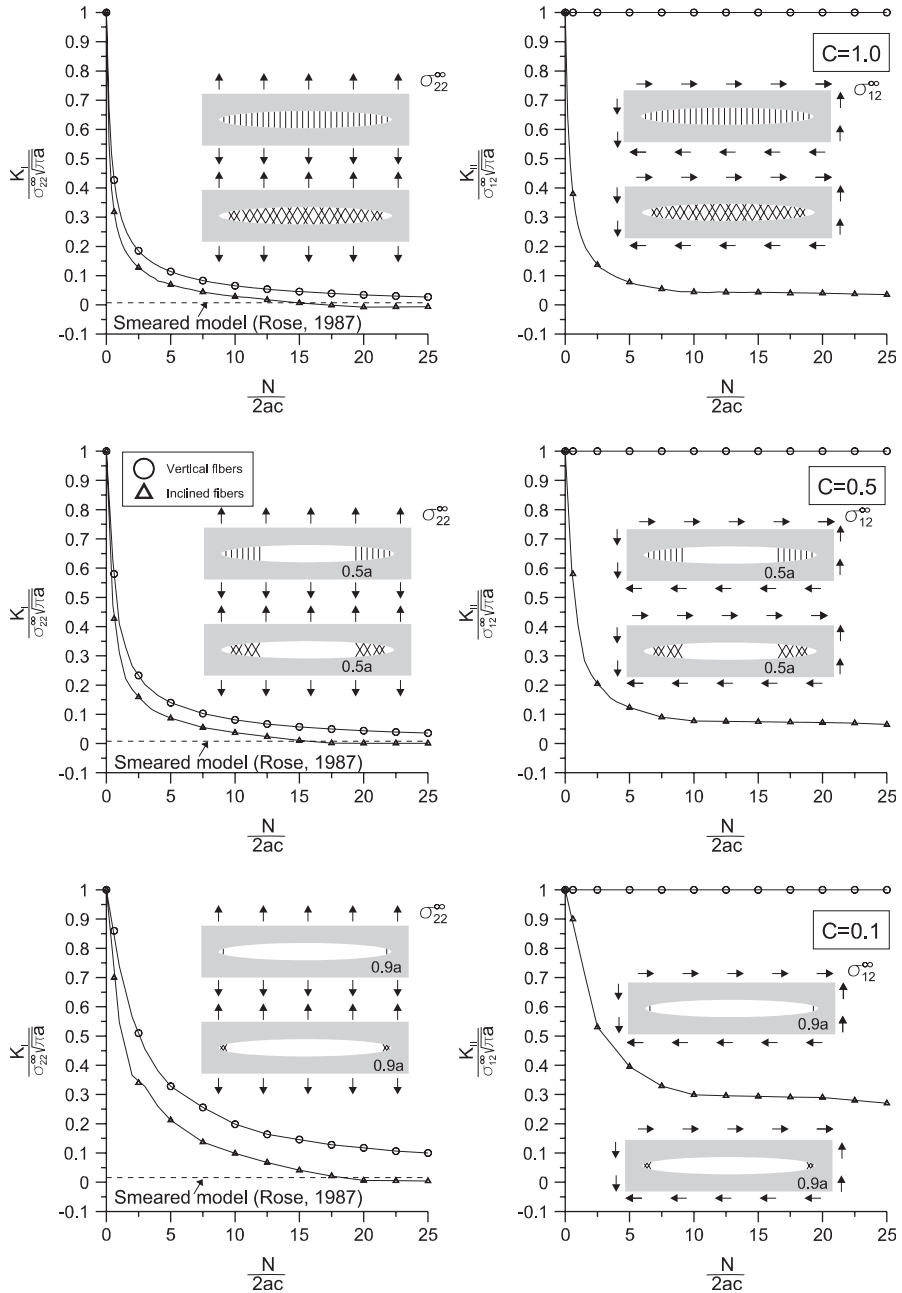
Fig. 11. Stress intensity factors K_I (left) and K_{II} (right) (normalized by $\sigma_{22}^\infty \sqrt{\pi a}$ and $\sigma_{12}^\infty \sqrt{\pi a}$) for an elliptical void having $a/b = 20$ reinforced by N fibers ($4N$ in the case of inclined fibers) with $\Lambda = 0.075$ ($\Lambda = 0.225$ in the case of inclined fibers) and loaded by far-field uniaxial (vertical) tensile stress and shear stress, respectively. Effect of morphology and number of fibers for full ($c = 1$, upper part), partial ($c = 0.5$, central part) and near-tip reinforcement ($c = 0.1$, lower part).

(corresponding to full reinforcement), $c = 0.5$ and $c = 0.1$ (corresponding to near-tip reinforcement). For the Mode I loading case, results are compared with similar results (but for a smeared fiber model) obtained by Rose (1987). This author has calculated that

$$\frac{K_I}{\sigma_{22}^\infty \sqrt{\pi a}} = \frac{1}{\sqrt{\pi c a h (2 - c)}}, \tag{30}$$

when

$$h = \frac{2k}{E'} \gg 1, \tag{31}$$

where E' is the reduced Young modulus, so that $E' = E$ for plane stress and $E' = E/(1 - v^2)$ for plane strain.

It is evident from Fig. 11 that

- an increase in fiber density relieves the stress at the tip;
- while the two bridging structures perform more or less equivalently for uniaxial remote tensile stress σ_{22}^∞, there is a strong difference under remote shear stress σ_{12}^∞;
- since the Rose model (valid for uniaxial tensile stress only) corresponds in essence to an infinite fiber density, the comparison of our discrete model with this reveals that *only a low fiber density (about $N/(2ac) = 15$) is needed to produce a stress relief nearly equal to that corresponding to the smeared (Rose) model*;
- for shear remote stress, vertical fibers do not affect the stress intensity factor;
- by comparing the cases $c = 1$, 0.5 and 0.1, it may be concluded that the fibers become particularly effective when located near the ends of the elliptical void (a conclusion consistent with our Section 4 findings for the two vertical fibers model).

Finally, level sets of the von Mises stress (normalized by σ_{22}^∞) are reported for different fiber densities and $c = 1$ in Fig. 12. In this figure, the number of fibers N has been taken equal to $\{0, 2, 4, 10, 20\}$ and $\{0, 8, 16, 40, 80\}$, respectively, in the left (vertical fibers case) and right part (inclined fibers case). It can be seen that the inclined fiber model provides greater stress relief around the elliptical void. The different behavior between the two different interface structures becomes even more evident when a remote shear stress is applied, Fig. 13. In this case the purely vertical fibers remain almost unstressed, providing essentially no stress relief.

4. Sharp crack reinforced by two symmetrical transverse fibers under Mode I

A sharp crack of length $2a$ is defined in the limit when axis b vanishes, $b = 0$. In this case, the near tip fields are obtained from Eqs. (17) in the limit $\rho \to 0$.

We consider now loading by a remote uniform stress σ_{22}^∞ and a reinforcing structure consisting of two fibers orthogonal to the fracture surfaces, with locations x and $-x$ from the central point of the crack (see the detail in Fig. 14). In this particular case, the traction distribution transmitted from the fibers to the matrix has only the normal component p different from zero, which, due to the Mode I symmetry, is proportional to the fiber elongation expressed simply as

$$p = 2k[u_2^\infty + p u_2^p]. \tag{32}$$
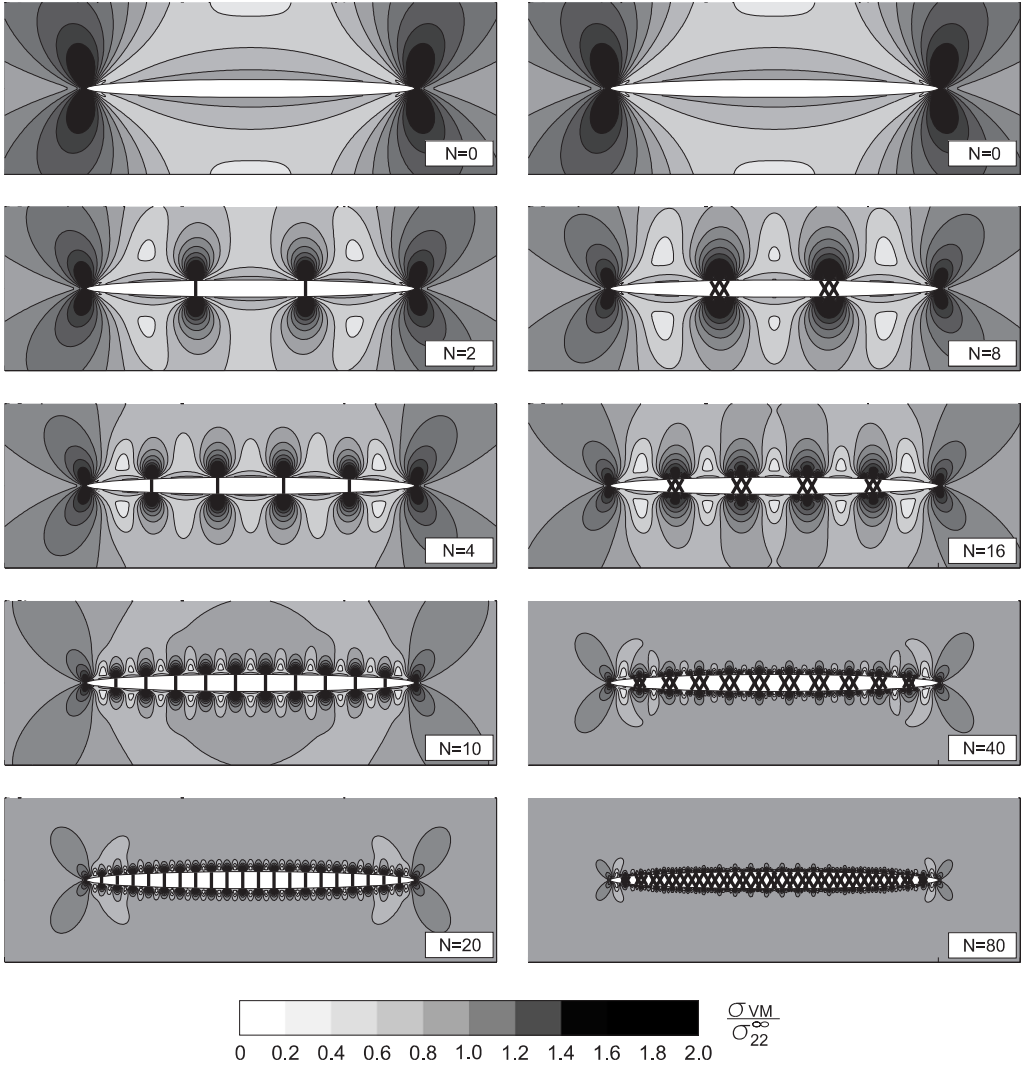
Fig. 12. Von Mises stress (normalized by remote stress) for an elliptical void ($a/b = 20$) reinforced by N fibers ($4N$ in the case of triangles) and loaded by a uniaxial vertical stress σ_{22}^{∞}. Parallel vertical fibers (left) and inclined fibers (right) are considered, characterized by the compliances $\Lambda = 0.075$ and 0.225, respectively.

In Eq. (32), u_2^{∞} is the displacement experienced by the junction central point (determined by $\beta \in [0, \pi/2]$ in the transformed plane of Fig. 7)

$$u_2^{\infty} = \frac{(1 + \kappa)a\sigma_{22}^{\infty} \sin \beta}{4\mu}, \tag{33}$$

due to the uniform remote stress σ_{22}^{∞}, and u_2^p is the displacement at the same point due to the four normal uniform traction distributions of unit magnitude applied over the four junction regions.
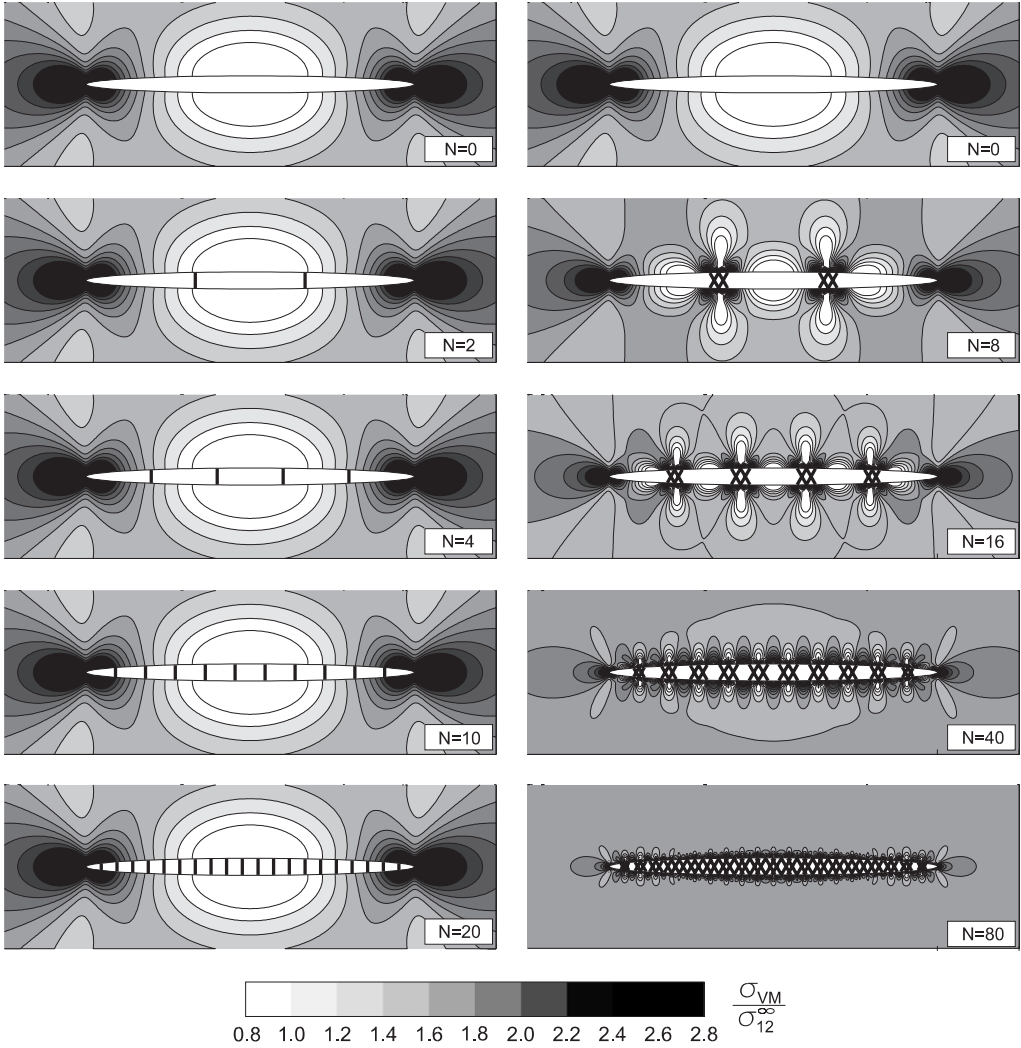
Fig. 13. Von Mises stress (normalized by remote stress) for an elliptical void ($a/b = 20$) reinforced with N fibers ($4N$ in the case of triangles) and loaded by a shear stress σ_{12}^{∞}. Parallel vertical fibers (left) and inclined fibers (right) are considered, characterized by the compliances $\Lambda = 0.075$ and 0.225, respectively. Note that, as expected, the vertical fibers remain unstressed, providing no stress relief.

A substitution of Eqs. (33) and (13) into Eq. (32) yields *the normal traction transmitted by the fibers to the matrix*, as a function of the (remote) loading σ_{22}^{∞} and the fiber position x, thickness t_b and stiffness k

$$p = a(1 + \kappa)k\pi\sigma_{22}^{\infty} \sin\beta \Big/ \left\{ 2\pi\mu - a(1 + \kappa)k \left[\cos\beta \log \left| \frac{\sin(\beta^+ - \beta)\sin(\beta^- + \beta)}{\sin(\beta^- - \beta)\sin(\beta^+ + \beta)} \right| \right.\right.$$
$$\left.\left. + \cos\beta^- \log \left| \frac{\sin\beta^- - \sin\beta}{\sin\beta^- + \sin\beta} \right| + \cos\beta^+ \log \left| \frac{\sin\beta^+ + \sin\beta}{\sin\beta^+ - \sin\beta} \right| - 2(\beta^+ - \beta^-)\sin\beta \right] \right\},$$

(34)
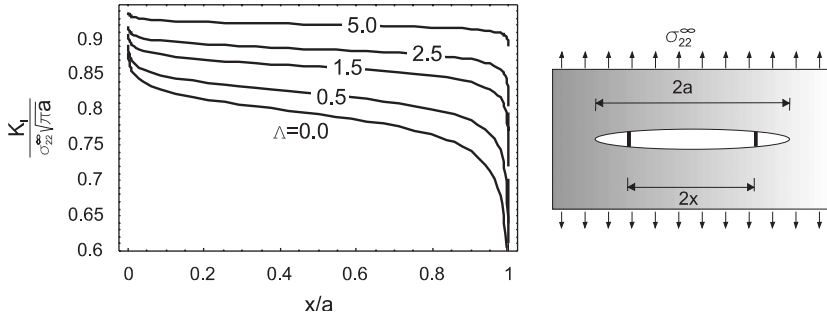
Fig. 14. Stress intensity factor K_I, normalized by $\sigma_{22}^\infty \sqrt{\pi a}$, for a sharp crack of length $2a$ reinforced by two symmetrical transverse fibers located at x and $-x$, for different values of the fibers' compliance parameter Λ.

where

$$\beta = \arccos\left(\frac{x}{a}\right), \quad \beta^- = \arccos\left(\frac{x}{a} + \frac{t_b}{2a}\right), \quad \beta^+ = \arccos\left(\frac{x}{a} - \frac{t_b}{2a}\right). \tag{35}$$

The stress intensity factor can now be obtained by substitution of Eq. (34) into Eq. (19). The variation of the stress intensity factor K_I (normalized by $\sigma_{22}^\infty \sqrt{\pi a}$) as a function of the fiber position x/a is shown in Fig. 14 for $t_b/a = \frac{1}{1000}$. Different values of the dimensionless fiber compliance parameter Λ are considered and we observe that the stress intensity factor tends to that corresponding to an unreinforced crack when Λ grows.

The most striking feature visible in Fig. 14 is that *the stress intensity factor decreases when the fibers approach the tips of the crack and, in particular, there is a huge drop, almost independent of the fiber stiffness, when x/a tends to 1.*

In particular, the stress intensity factor is null for

$$\Lambda = \frac{a}{\pi t_b} \left[\cos\beta \log\left|\frac{\sin(\beta^+ - \beta)\sin(\beta^- + \beta)}{\sin(\beta^- - \beta)\sin(\beta^+ + \beta)}\right| \right.$$
$$\left. + \cos\beta^- \log\left|\frac{\sin\beta^- - \sin\beta}{\sin\beta^- + \sin\beta}\right| + \cos\beta^+ \log\left|\frac{\sin\beta^+ + \sin\beta}{\sin\beta^+ - \sin\beta}\right| \right], \tag{36}$$

which turns out to be positive for $x/a \to 1$. We can therefore conclude that a fiber of the appropriate stiffness (given by Eq. (36)) at the crack tip makes the stress singularity null, a circumstance in agreement with the Dugdale–Barenblatt model (1960, 1962).

In the special case of a single central fiber, i.e. for $x = 0$, Eq. (34) reduces to

$$p = \frac{2a(1 + \kappa)k\pi\sigma_{22}^\infty}{4\pi\mu + (\kappa + 1)k[2a(\pi - 2\arccos(t_b/2a)) + t_b \log |(\sqrt{4a^2 - t_b^2} + 2a)/(\sqrt{4a^2 - t_b^2} - 2a)|]}, \tag{37}$$

a situation also analyzed by Rubinstein (1994). In particular, the stress intensity factor (made dimensionless by division by $\sigma_{22}^\infty \sqrt{\pi t_b}$) and the traction transmitted by the fiber to the matrix are plotted in Fig. 15, for different values of the stiffness parameter Λ as a function of the fiber spacing aspect ratio $(2a - t_b)/2t_b$. These results appear to be identical to those given by Rubinstein (1994, Fig. 2).
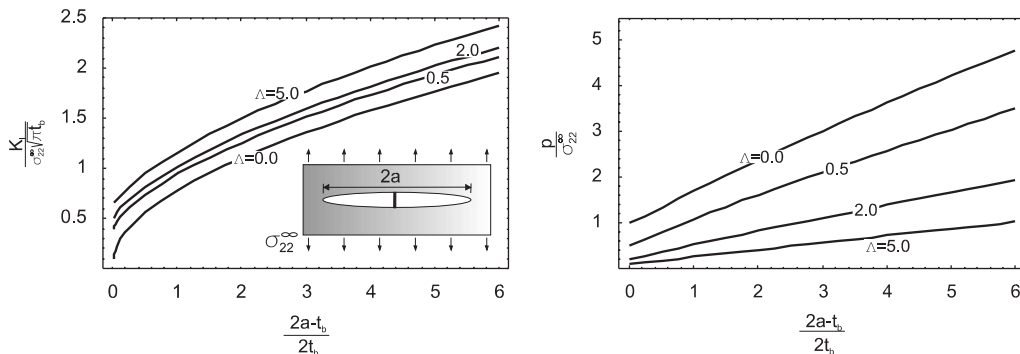
Fig. 15. Stress intensity factor (left) and traction transmitted by the fiber to the matrix (right) for a single transverse central fiber, for different values of the fibers stiffness parameter Λ.

5. Conclusions

We have shown that the model of a structural interface developed by Bigoni and Movchan (2002) and Bertoldi et al. (2007a, b) is a powerful tool to investigate cracks and elliptical voids bridged by fibers. In particular, we have provided for the first time: (i) the full-field solution for an elliptical void reinforced by an arbitrary (even random) fiber distribution; (ii) the stress intensity factor for a bridged crack or a thin, bridged elliptical void, accounting for fibers' inclination and distribution. The solutions demonstrate the effects of fibers' geometry and stiffness. For instance, we have shown that a fiber (of appropriate stiffness) orthogonal to the crack and very near the crack tip can reduce the stress intensity to zero. On the other hand, a fiber almost parallel to the crack axis can increase the stress intensity factor beyond 1. Fig. 10 shows an optimal fiber distribution (for centered fibers) to minimize the stress intensity factor both for Mode I and Mode II loadings.

Acknowledgments

References

Barenblatt, G.I., 1962. The mathematical theory of equilibrium of cracks in brittle fracture. Adv. Appl. Mech. 9, 55–129.

Bertoldi, K., Bigoni, D., Drugan, W.J., 2007a. Structural interfaces in linear elasticity. Part I: nonlocality and gradient approximations. J. Mech. Phys. Solids 55 (1), 1–34.

Bertoldi, K., Bigoni, D., Drugan, W.J., 2007b. Structural interfaces in linear elasticity. Part II: effective properties and neutrality. J. Mech. Phys. Solids 55 (1), 35–63.

Bigoni, D., Movchan, A.B., 2002. Statics and dynamics of structural interfaces in elasticity. Int. J. Solids Struct. 39, 4843–4865.

Creager, M., Paris, P.C., 1967. Elastic field equations for blunt cracks with reference to stress corrosion cracking. Int. J. Fract. Mech. 3, 247–252.

Dugdale, D.S., 1960. Yielding of steel sheets containing slits. J. Mech. Phys. Solids 8, 100–104.

Kozlov, V.A., Maz'ya, V.G., Movchan, A.B., 1999. Asymptotic Analysis of Fields in Multi-structures. Oxford University Press, Oxford.

Meda, G., Steif, P.S., 1992. Analysis of a crack bridged by a single fiber. J. Appl. Mech. 59, 524–529.

Movchan, A.B., Willis, J.R., 1993. Asymptotic analysis of the reinforcement of a brittle crack by bridging fibers. Q. J. Mech. Appl. Math. 46, 331–350.

Movchan, N.V., Willis, J.R., 1996. Critical load for a Mode-I crack reinforced by bridging fibres. Q. J. Mech. Appl. Math. 49, 545–564.

Movchan, N.V., Willis, J.R., 1997. Asymptotic analysis of reinforcement by frictional fibres. Proc. R. Soc. London 453, 757–784.

Muskhelishvili, N.I., 1953. Some basic problems of the mathematical theory of elasticity. Groningen, Holland: Noordhoff.

Rose, L.R.F., 1987. Crack reinforcement by distributed springs. J. Mech. Phys. Solids 35, 383–405.

Rubinstein, A.A., 1994. Strength of fiber reinforced ceramics on the basis of a micromechanical analysis. J. Mech. Phys. Solids 42, 401–422.